

Enhanced Rotation of the Polarization of a Light Beam Transmitted through a Silver Film with an Array of Perforated S-Shaped Holes

Shan Wu,^{1,2} Zhao Zhang,¹ Yi Zhang,¹ Kaiyin Zhang,² Lin Zhou,¹ Xuejin Zhang,^{1,*} and Yongyuan Zhu^{1,†}

¹National Laboratory of Solid State Microstructures, National Center of Microstructures and Quantum Manipulation, Nanjing University, Nanjing 210093, China

²Department of Physics, Fuyang Normal College, Fuyang, Anhui 236032, China

(Received 22 January 2013; published 13 May 2013)

In this Letter, we realized an enhanced optical rotation of the zero-order transmitted light through a silver film with an array of perforated S-shaped holes. Different from the previous studies, this effect results from the contribution of both the localized surface plasmons and surface plasmon polaritons (SPPs). The rotation angle can be modulated with the thickness due to the phase retardation of the SPPs when tunneling to the emitted surface. With a sample thickness 245 nm, a near-complete cross-polarization conversion (90° optical rotation) can be achieved, representing a major advance in performance compared to the previously reported planar chiral structures.

DOI: [10.1103/PhysRevLett.110.207401](https://doi.org/10.1103/PhysRevLett.110.207401)

PACS numbers: 78.66.Bz, 41.20.Jb, 78.20.Ek, 78.67.Bf

Polarization is an important characteristic of light due to many phenomena inherently polarization sensitive. The capability of manipulating the polarization state is of high interest for many applications such as polarization controllers and circular polarizers for optoelectronic, life science microscopy, and display applications [1]. Currently, manipulating polarization may be realized using anisotropic or chiral materials, but with specific thickness limitations and quite bulky configurations [2]. In order to realize the miniaturization of the devices, some microstructures, such as artificial planar chiral structures, [3–9] plasmonic crystals, [10] spiral bull-eye structures, [11–15] 3D metamaterials [16,17], and other planar nonchiral metamaterials, [18,19] have been widely investigated experimentally and theoretically. For example, Papakostas *et al.* [4] have observed polarization conversion by metallic gammadion arrays and found a rotation in excess of 30° in the nonzero-order diffraction. Unfortunately, for zero-order transmission only a small rotation can be realized ($\sim 2^\circ$) with most planar chiral structures [5], which limits its applications. For achieving a high rotation in zero-order transmission, some multilayer chiral structures are designed and experimented [20–24]. For instance, Ye observed a 90° rotation of a bilayered chiral metamaterial in the microwave range using the transverse magnetic dipole coupling effects [24]. For the optical rotation of the single-layer structures, the observed optical rotations are mainly in nonzero-order diffraction.

On the other hand, the periodic perforated metallic structures supporting the surface plasmon polaritons (SPPs) and localized surface plasmons (LSPs) resonances can bring an enhanced zero-order optical transmission [25,26]. People expect to achieve the higher optical rotation utilizing this effect. However, the general nanohole structures only supporting the SPPs resonances cannot produce optical rotation. If the sample has a broken symmetry the optical rotation

can be realized. For example, by introducing broken time-reversal symmetry [27], the polarization conversion can be achieved through dissipative coupling in plasmonic nanostructures mimicking the quantum “Hanle effect”. For the structure broken metallic samples [28–31], such as the L-shaped nanohole arrays, due to the excitation of the LSPs resonances, the induced charges would be displaced not only along the direction of the incident field, but also into another direction through the bent corner of L (we call it charge transfer), thereby resulting in a polarization perpendicular to the driving electric field. Based on the superposition principle, the polarization of the zero-order transmitted light would rotate. However, due to the limitation of charge transfer, the polarization rotation angle for a single-layer metallic structure cannot exceed 45°. A larger rotation than 45° would require multilayer structures [32].

In this Letter, we point out that if the SPPs and LSPs resonances can be excited simultaneously, utilizing the phase change of the SPPs on the emitted surface, a higher optical rotation can be expected with a single-layer perforated metallic structure. By careful design, an enhanced optical rotation in the zero-order transmission through a silver film with an array of perforated S-shaped holes has been achieved experimentally and theoretically. Increasing the thickness of the metallic film to 245 nm would result in a near-complete cross-polarization conversion (90°). Comparing to the conventional planar chiral structures, it has not only a high optical rotation but also strong transmission.

For the conventional optical rotation exhibited by chiral molecules, the rotation effect results from the presence of both electric and magnetic responses. It requires that an electric (magnetic) dipole moment induced in the molecule be parallel to the incident magnetic (electric) field. The oscillating electric (magnetic) dipole emits an electromagnetic wave with its polarization perpendicular to the incident light. Their phase difference and amplitude decides

the optical polarization rotation ϕ and ellipticity e ($e = a/b$, here, a and b are the short and long semiaxes of the polarization ellipse). In our proposed structure, the polarization rotation is due to the superposition of electromagnetic waves emitted by the LSPs and SPPs resonances. Its physical mechanism is as follows. When an x -polarized wave is incident normally to the sample, the electric field of the transmitted light can be written as

$$\begin{aligned} \vec{E}^{\text{out}}(r, t) &= \vec{E}_x + \vec{E}_y \\ &= E_x \cos(kz - \omega t + \varphi_x) \vec{x} + E_y \cos(kz - \omega t + \varphi_y) \vec{y}, \end{aligned} \quad (1)$$

where $\vec{E}_x = \vec{E}_{\text{LSP}x} + \vec{E}_{\text{SPP}x}$ and $\vec{E}_y = \vec{E}_{\text{LSP}y} + \vec{E}_{\text{SPP}y}$, \vec{E}_{SPP} and \vec{E}_{LSP} are the electric field of the electromagnetic wave related to the SPPs and LSPs resonances. Utilizing the well-known equation

$$\frac{x^2}{E_x^2} + \frac{y^2}{E_y^2} - 2 \frac{\cos \delta}{E_x E_y} xy = \sin^2 \delta, \quad (2)$$

where the phase difference $\delta = \varphi_y - \varphi_x$, we can obtain the transmitted polarization state. In general, a linearly polarized wave transmitted through the structure will become elliptical [1]. When $0 < \delta < \pi$, the polarization state is left handed, which corresponds to a clockwise rotation of the electric field vector in the xy plane. However, when $\pi < \delta < 2\pi$, instead, it is right handed. For the LSPs resonances, the induced charges have a collective oscillation on whole nanohole walls. Thus, the amplitudes of the electric fields at the input and output surfaces are the same (see the Supplemental Material S1 [33]). Generally, the SPPs resonances cannot produce the optical rotation effect, i.e., $\vec{E}_{\text{SPP}y} = 0$. However, when tunneling to the emitted surface through the nanoholes, the SPPs waves excited on the incident surface acquire a phase variation $\Delta\Phi = \beta z_{z=d} - \beta z_{z=0} = \beta d$, where β and d are the propagating constant of the SPPs in the nanohole and the metallic film thickness, respectively. By manipulating the $\Delta\Phi$ through the sample thickness, the polarization of transmitted light can be controlled. Further, if $\vec{E}_x = \vec{E}_{\text{LSP}x} + \vec{E}_{\text{SPP}x} = 0$, a near-complete cross-polarization conversion (90°) can be obtained.

The schematic diagram of the designed sample structures and its geometrical parameters are shown in Fig. 1, where $w = 60$ nm, $R = 420$ nm, $\alpha = 88^\circ$, and the period $p = 680$ nm. In the experiment, a 100 nm thick silver film was sputtered on a 1 mm thick SiO_2 substrate. The structures of the metallic film were milled with the focused ion beam (FIB) system (strata FIB 201, FEI Co. 30 keV Ga ions). The lower-right inset of Fig. 1 is the FIB image. In the polarization rotation investigation, the sample was planted on a home-built optical setting with an illumination of a 50 W halogen lamp. A linearly polarized light was incident normally to the sample plane after being slightly

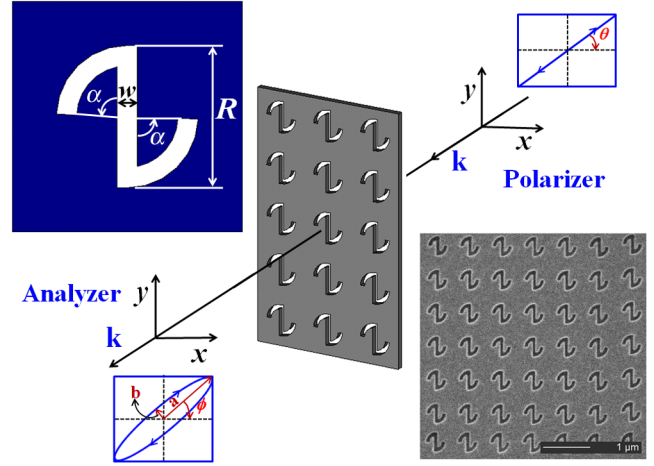


FIG. 1 (color online). Schematic of the experimental setup of the polarized transmission analyses for any given polarizer incidence after the sample. Upper-left inset is the designed one unit cell, and lower-right inset is a typical FIB image of the sample, where the structural parameters are $w = 60$ nm, $R = 420$ nm, $\alpha = 88^\circ$, and $P = 680$ nm. In the experiment, the incident light remains a linear polarization along the x axis ($\theta = 0^\circ$).

focalized by a convex lens. The zero-order transmission was collected by an optical spectrum analyzer (ANDO AQ-6315) via a polarization analyzer. The schematic of experimental setup is shown in Fig. 1.

In the measurement, the incident light was x polarized ($\theta = 0^\circ$). By tuning the polarization analyzer, the optical transmission can be recorded in any preferred polarization angle ϕ . We use ϕ_{max} representing the optical rotation angle corresponding to the maximum transmittance (i.e., the angle between the long axis of the transmitted polarization ellipse and the incident polarization direction). Figure 2(a) shows the transmission spectra with the different ϕ . There are two transmission peaks at wavelength about 875 and 1110 nm. For the peak 875 nm, the measured ϕ_{max} is -27° and its rotary power ρ (ρ is defined by the rotation angle per unit length) reaches up to 2.7×10^5 deg/mm. However, for the peak 1110 nm, $\phi_{\text{max}} = -41^\circ$ and $\rho = 4.1 \times 10^5$ deg/mm. Their corresponding effective circular birefringence $\Delta n = |n_l - n_r| = \rho \lambda / \pi = 1.3$ and 2.53 are much larger than that of quartz ($\Delta n = 6.6 \times 10^{-5}$ at wavelength 632.8 nm) [34], where n_l and n_r are the effective refractive index of left and right circularly polarized light, respectively.

The optical transmission of our designed sample was calculated using the finite-difference time-domain method [35]. The dielectric constant of glass substrate is ϵ_g set as 2.2 and the silver ϵ_m is modeled by the Drude model, with the plasma frequency of 1.374×10^{16} rad/s and collision frequency of 2.02×10^{14} rad/s. The calculated results are shown in Fig. 2(b), which agree with the experimental results. Corresponding to the experimental transmission peaks, the calculated peaks are 868 and 1089 nm, whose

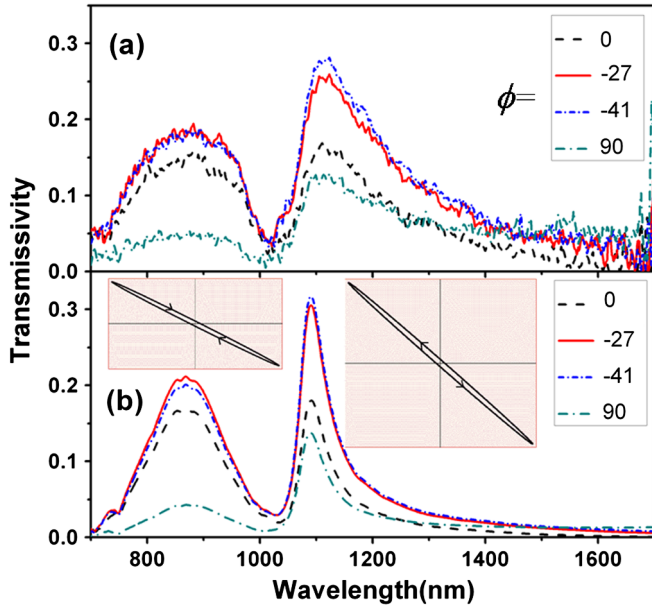


FIG. 2 (color online). (a), (b) The experimental and calculated optical transmission with different analyzer angle ϕ . The largest transmission spectra of the peak 868 nm occurs at $\phi_{\max} = -27^\circ$ and peak 1089 nm occurs at $\phi_{\max} = -41^\circ$. The insets of (b) are the elliptical polarization states of two resonance peaks.

polarization states are left handed and right handed, respectively [Fig. 2(b)]. Their ellipticities e are 0.026 and 0.027.

In practical application, a 90° polarization rotation is preferred. Generally, for natural chiral media, the polarization rotation angle has a linear increase with the thickness of the sample. Here, we also hope to obtain a high rotation angle through increasing the sample thickness. We mainly discuss the optical rotation of the resonance peak around 1089 nm. The calculated results are shown in Fig. 3(a). Quite different from the conventional chiral media, the polarization rotation angle has a nonlinear increasing trend. With a thickness of metallic film 245 nm, a near 90° optical rotation can be achieved with a nearly linear polarization state ($e = 0.0078$). When normalized with open areas, the transmission is up to 132.7%, much larger than the classic Bethe theoretical limits [Fig. 3(b)].

In order to verify whether the polarization rotation is due to the superposition of electromagnetic waves emitted by the LSPs and SPPs resonances, we calculated the optical rotation at wavelength range 1000–3000 nm. Figures 4(a) and 4(b) are the x and y components of the electric field (E_x and E_y) detected by the probe at the far field with different sample thickness (100 and 245 nm). There are two peaks (denoted by peaks 1 and 2) in the transmission spectra. It can be clearly seen that peak 1 is dependent on the thickness while peak 2 is not. Figures 5(a) and 5(b) are their electric field (E_x and E_y) distributions along the x direction on the emitted (air-metal) surface with the sample thickness of 245 nm. Here, the E_x components in the zones (1) E_{x1} and (2) E_{x2} result from the LSPs and SPPs resonances;

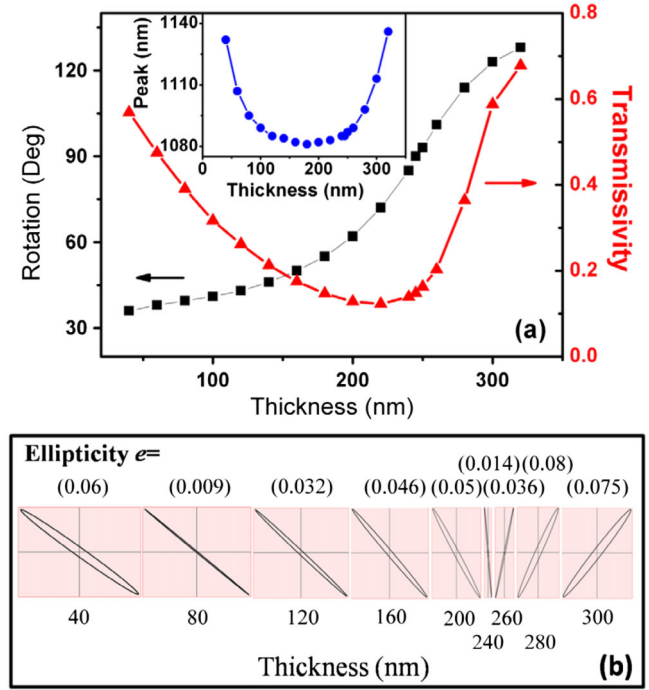


FIG. 3 (color online). (a) The dependence of the polarization rotation angle (black square line) and transmissivity (red triangle line) and wavelength of the peak (blue circle line in the inset) on the thickness of the metallic film. (b) The elliptical polarization states and the corresponding ellipticities for the different thicknesses.

however, the E_y components in zone (1) E_{y1} only result from the LSPs resonances (here $E_{y2} \approx 0$, because the SPPs can not produce the E_y components). Peak 1 is attributed to both the SPPs (1,0) resonances in glass-metal surface and

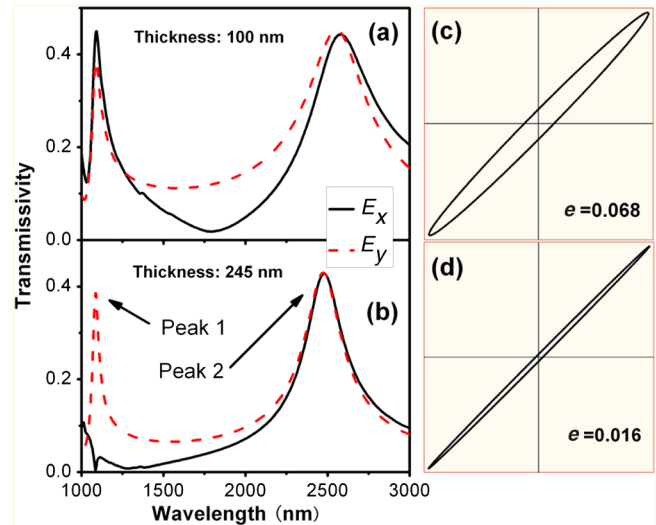


FIG. 4 (color online). (a), (b) The calculated electric field E_x (black solid line) and E_y (red dashed line) components of the transmitted light with different sample thickness. (c), (d) The elliptical polarization states of peak 2 with the sample thickness of 100 (c) and 245 nm (d), respectively.

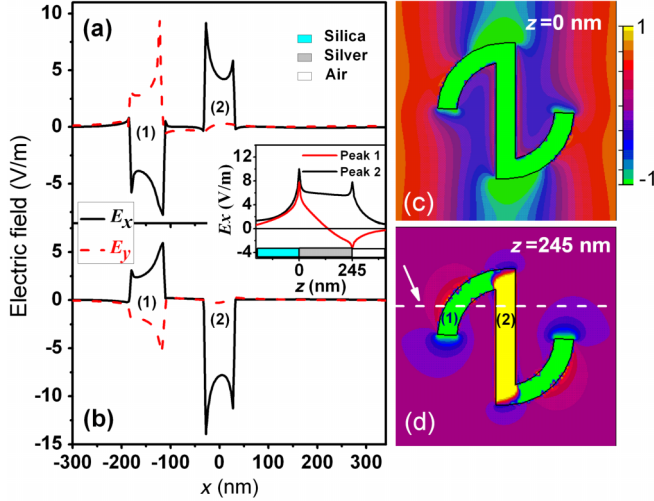


FIG. 5 (color online). (a), (b) The electric field E_x (black solid line) and E_y (red dashed line) components of peak 1 and 2 on the emitted surface ($z = 245$ nm) along the white dashed line in (d). Mark (1) and (2) correspond to the zones (1) and (2) in (d). The inset shows the E_x components of peak 1 (red line) and 2 (black line) along the z direction at the center of the unit cell. (c), (d) The electric field E_x distribution of the peak 1 on the incident ($z = 0$ nm) and emitted ($z = 245$ nm) surface, respectively.

the electric quadrupolar LSPs resonances [36]. The inset of Figs. 5 is the E_x components of peaks 1 and 2 along the z direction at the center of the unit cell. It can be seen that for the peak 1 the E_x component at the two sample's surface ($z = 0$ nm and 245 nm) have an opposite sign due to the phase retardation of the SPPs waves. Consequently, on the emitted surface, the E_{x1} component in the zone (1) has almost the same amplitude as the E_{x2} in the zone (2) but with the opposite sign (Fig. 5(a) and Supplemental Material S1 [33]). These act as two dipoles whose emitted electromagnetic waves interfere destructively in the far field, resulting in a near-zero E_x component [Fig. 4(b)]. However, the E_y components coming from the LSPs resonances (E_{LSPy}) remain unchanged [Figs. 4(a), 4(b), and 5(a)]. Based on the above discussions, a near-complete cross-polarization rotation appears. The electric field E_x distributions in Figs. 5(c) and 5(d) also testify to this point. At the incident surface ($z = 0$ nm), the E_{x1} and E_{x2} components have the same sign. However, due to the phase retardation of the SPPs waves, on the emitted surface ($z = 245$ nm), the E_{x1} and E_{x2} components have the opposite sign. On the other hand, peak 2 is far from the SPPs resonances; therefore, it can only be attributed to the dipolar LSPs resonances. As a result, the E_{x2} components on the two surfaces have the same sign [inset of Fig. 5]. Thus, at the emitted surface, the amplitudes of the E_x and E_y components almost keep constant with the thickness [see Figs. 4(a) and 4(b), and Supplemental Material S1]. Through superposition a transmitted light with a 41° polarization can be obtained. Its rotation angle remains

unchanged with the thickness except the resonance peak has a slight shift and its ellipticity changes from 0.068 to 0.016 [Figs. 4(c) and 4(d)].

Here, the proposed metallic nanohole structures with the enhanced optical rotation are different from the widely studied planar chiral structures with the C_4 (fourfold rotational) symmetry about the z axis. The polarization rotation results from the superposition of the electromagnetic waves emitted by the LSPs and SPPs resonances. As long as the metallic structures can supply the E_y components through the LSPs resonances, utilizing the phase retardation of the SPPs wave, one can get any desired optical rotation polarization states. This kind of effect can obtain higher rotation than that of the metallic planar chiral structures. For example, we also investigated other metallic nanohole structures. Figure 6 shows the experimental and calculated results of the periodic metallic M -shaped nanohole structures. Its geometric parameters are defined in the inset of Fig. 6(b). The results exhibit a right-handed polarization resonance characteristic at wavelength of about 1091 nm, where the optical polarization rotation angle and ellipticity is -42° and 0.073, respectively.

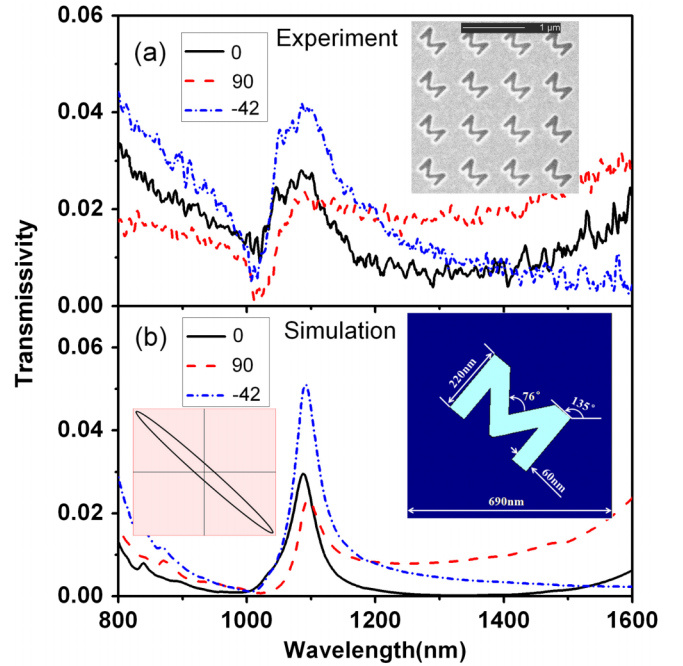


FIG. 6 (color online). (a), (b) The experimental and calculated transmission spectra of M -shaped metallic nanohole structures. The incident light polarization is along the x axis ($\theta = 0^\circ$). Black solid, red dashed, and blue short dashed-dotted lines represent the transmission spectra of the analyzer $\phi = 0^\circ$, 90° , -42° , respectively. The inset of (a) is the experimental FIB image. The insets of (b) are the corresponding elliptical polarization state and schematic diagram of the unit cell with the geometric parameters. The thickness of the metallic film is 100 nm.

In conclusion, we have theoretically and experimentally demonstrated enhanced optical polarization rotation in single-layer metallic nanohole arrays. Different from previous studies, this effect arises from the superposition of electromagnetic waves radiated by LSPs and SPPs modes. Through changing the sample thickness, any desired rotation angles can be achieved. With a sample thickness 245 nm, a near-complete cross-polarization conversion in the zero-order transmission can be achieved. Our results can be straightforwardly applied to the realization of miniaturized optical systems based on optical polarization rotation metamaterials.

This work was supported by the State Key Program for Basic Research of China (Grants No. 2010CB630703 and No. 2012CB921502) and by the National Natural Science Foundation of China (Grants No. 11104032, No. 51271059, No. 11274159 and No. 11174128) and by Anhui Provincial Natural Science Foundation (Grant No. 10040606Q48) and PAPD.

*xuejinzh@nju.edu.cn

†yyzhu@nju.edu.cn

- [1] A. V. Rogacheva, V. A. Fedotov, A. S. Schwanecke, and N. I. Zheludev, *Phys. Rev. Lett.* **97**, 177401 (2006).
- [2] Y. Zhao and A. Alù, *Phys. Rev. B* **84**, 205428 (2011).
- [3] A. S. Schwanecke, A. Krasavin, D. M. Bagnall, A. Potts, A. V. Zayats, and N. I. Zheludev, *Phys. Rev. Lett.* **91**, 247404 (2003).
- [4] A. Papakostas, A. Potts, D. M. Bagnall, S. L. Prosvirnin, H. J. Coles, and N. I. Zheludev, *Phys. Rev. Lett.* **90**, 107404 (2003).
- [5] T. Vallius, K. Jefimovs, J. Turunen, P. Vahimaa, and Y. Svirko, *Appl. Phys. Lett.* **83**, 234 (2003).
- [6] W. Zhang, A. Potts, A. Papakostas, and D. M. Bagnall, *Appl. Phys. Lett.* **86**, 231905 (2005).
- [7] M. Kuwata-Gonokami, N. Saito, Y. Ino, M. Kauranen, K. Jefimovs, T. Vallius, J. Turunen, and Y. Svirko, *Phys. Rev. Lett.* **95**, 227401 (2005).
- [8] S. L. Prosvirnin and N. I. Zheludev, *Phys. Rev. E* **71**, 037603 (2005).
- [9] B. F. Bai, Y. Svirko, J. Turunen, and T. Vallius, *Phys. Rev. A* **76**, 023811 (2007).
- [10] J. Elliott, I. I. Smolyaninov, N. I. Zheludev, and A. V. Zayats, *Phys. Rev. B* **70**, 233403 (2004).
- [11] P. Genevet, J. Lin, M. A. Kats, and F. Capasso, *Nat. Commun.* **3**, 1278 (2012).
- [12] A. Drezet, C. Genet, J. Y. Laluet, and T. W. Ebbesen, *Opt. Express* **16**, 12 559 (2008).
- [13] A. Drezet, C. Genet, and T. W. Ebbesen, *Phys. Rev. Lett.* **101**, 043902 (2008).
- [14] E. Lombard, A. Drezet, C. Genet, and T. W. Ebbesen, *New J. Phys.* **12**, 023027 (2010).
- [15] Y. Gorodetski, E. Lombard, A. Drezet, C. Genet, and T. W. Ebbesen, *Appl. Phys. Lett.* **101**, 201103 (2012).
- [16] J. K. Gansel, M. Thiel, M. S. Rill, M. Decker, K. Bade, V. Saile, G. von Freymann, S. Linden, and M. Wegener, *Science* **325**, 1513 (2009).
- [17] J. K. Gansel, M. Latzel, A. Frölich, J. Kaschke, M. Thiel, and M. Wegener, *Appl. Phys. Lett.* **100**, 101109 (2012).
- [18] J. M. Hao, Y. Yuan, L. X. Ran, T. Jiang, J. A. Kong, C. T. Chan, and L. Zhou, *Phys. Rev. Lett.* **99**, 063908 (2007).
- [19] E. Plum, X. X. Liu, V. A. Fedotov, Y. Chen, D. P. Tsai, and N. I. Zheludev, *Phys. Rev. Lett.* **102**, 113902 (2009).
- [20] D. H. Kwon, P. L. Werner, and D. H. Werner, *Opt. Express* **16**, 11 802 (2008).
- [21] M. Decker, M. W. Klein, M. Wegener, and S. Linden, *Opt. Lett.* **32**, 856 (2007).
- [22] E. Plum, J. Zhou, J. Dong, V. A. Fedotov, T. Koschny, C. M. Soukoulis, and N. I. Zheludev, *Phys. Rev. B* **79**, 035407 (2009).
- [23] R. Zhao, L. Zhang, J. Zhou, T. Koschny, and C. M. Soukoulis, *Phys. Rev. B* **83**, 035105 (2011).
- [24] Y. Q. Ye and S. L. He, *Appl. Phys. Lett.* **96**, 203501 (2010).
- [25] T. W. Ebbesen, H. J. Lezec, H. F. Ghaemi, T. Thio, and P. A. Wolff, *Nature (London)* **391**, 667 (1998).
- [26] S. Wu, Q. J. Wang, X. G. Yin, J. Q. Li, D. Zhu, S. Q. Liu, and Y. Y. Zhu, *Appl. Phys. Lett.* **93**, 101113 (2008).
- [27] P. Ginzburg, F. J. Rodríguez-Fortuño, A. Martínez, and A. V. Zayats, *Nano Lett.* **12**, 6309 (2012).
- [28] T. Li, H. Liu, S. M. Wang, X. G. Yin, F. M. Wang, S. N. Zhu, and X. Zhang, *Appl. Phys. Lett.* **93**, 021110 (2008).
- [29] N. Yu, P. Genevet, M. A. Kats, F. Aieta, J. P. Tetienne, F. Capasso, and Z. Gaburro, *Science* **334**, 333 (2011).
- [30] F. Aieta, A. Kabiri, P. Genevet, N. Yu, M. A. Kats, Z. Gaburro, and F. Capasso, *J. Nanophoton.* **6**, 063532 (2012).
- [31] P. Genevet, N. Yu, F. Aieta, J. Lin, M. A. Kats, R. Blanchard, M. O. Scully, Z. Gaburro, and F. Capasso, *Appl. Phys. Lett.* **100**, 013101 (2012).
- [32] T. Li, S. M. Wang, J. X. Cao, H. Liu, and S. N. Liu, *Appl. Phys. Lett.* **97**, 261113 (2010).
- [33] See Supplemental Material at <http://link.aps.org/supplemental/10.1103/PhysRevLett.110.207401> for details concerning the electric field E_x and E_y distributions of peaks 1 and 2 on the incident ($z = 0$ nm) and emitted ($z = 245$ nm) surfaces of the sample.
- [34] A. Yariv and P. Yeh, *Optical Waves in Crystals* (Wiley, New York, 1984).
- [35] D. M. Sullivan, *Electromagnetic Simulation Using the FDTD Method* (IEEE, New York, 2000).
- [36] S. Wu, J. Q. Liu, L. Zhou, Q. J. Wang, Yi. Zhang, G. D. Wang, and Y. Y. Zhu, *Appl. Phys. Lett.* **99**, 141104 (2011).